Sub-wavelength waveguide loaded by a complementary electric metamaterial for vacuum electron devices

Citation: Duan, Zhaoyun, et al. "Sub-Wavelength Waveguide Loaded by a Complementary Electric Metamaterial for Vacuum Electron Devices." Physics of Plasmas 21, 10 (October 2014): 103301 © 2014 AIP Publishing

As Published: http://dx.doi.org/10.1063/1.4897392

Publisher: American Institute of Physics (AIP)

Persistent URL: http://hdl.handle.net/1721.1/111190

Version: Author's final manuscript: final author's manuscript post peer review, without publisher's formatting or copy editing

PSFC/JA-14-46

Sub-wavelength Waveguide Loaded by a Complementary Electric Metamaterial for Vacuum Electron Devices

Duan, Z., Hummelt, J.S., Shapiro, M.A., Temkin, R.J.

December, 2014

Plasma Science and Fusion Center
Massachusetts Institute of Technology
Cambridge MA 02139 USA

This work was supported by AFOSR MURI under Grant No. FA9550-12-1-0489.

Sub-wavelength waveguide loaded by a complementary electric metamaterial for vacuum electron devices

Duan, Z., Hummelt, J.S., Shapiro, M.A, Temkin, R.J.

We report the electromagnetic properties of a waveguide loaded by complementary electric split ring resonators (CeSRRs) and the application of the waveguide in vacuum electronics. The S-parameters of the CeSRRs in free space are calculated using the HFSS code and are used to retrieve the effective permittivity and permeability in an effective medium theory. The dispersion relation of a waveguide loaded with the CeSRRs is calculated by two approaches: by direct calculation with HFSS and by calculation with the effective medium theory; the results are in good agreement. An improved agreement is obtained using a fitting procedure for the permittivity tensor in the effective medium theory. The gain of a backward wave mode of the CeSRR-loaded waveguide interacting with an electron beam is calculated by two methods: by using the HFSS model and traveling wave tube theory; and by using a dispersion relation derived in the effective medium model. Results of the two methods are in very good agreement. The proposed all-metal structure may be useful in miniaturized vacuum electron devices.

1. Introduction

Since a left-handed medium was first realized in 2000 [1], researchers worldwide have been interested in its exotic electromagnetic properties such as negative refractive index [2, 3], backward Cerenkov radiation [2, 4] and the realization of different types of metamaterials (MTMs) and their potential applications.

Rectilinear electron beams interacting with slow waves in periodic structures are used in traveling wave tubes (TWTs) or backward wave oscillators (BWOs). An interaction circuit of a TWT or BWO can be designed as a helix, coupled-cavity structure, folded waveguide or ladder structure depending on the frequency range [5-7]. MTMs and photonic crystals built of metallic parts can be considered as modified coupled-cavity or ladder structures and are promising for application in TWTs or BWOs. The wave-electron beam interaction in MTMs has been theoretically studied in [8-15]. Here we focus on the MTM-loaded waveguide and its application as an interaction circuit for a vacuum electron device.

Waves in the MTM-loaded waveguide can be described using different models. The MTM-loaded rectangular waveguide was theoretically studied as early as 2001 [16]. Subsequently, Marques *et al*. reported a split ring resonator (SRR)-loaded waveguide and verified its transmission characteristics in experiment when the waveguide operates below the cutoff frequency of the TE mode [17]. It has been shown that the cutoff waveguide provides negative permittivity and the SRRs offer negative permeability, which, therefore, explains wave propagation in the SRR-loaded waveguide. Esteban *et al*. showed that a rod-loaded waveguide supports an electromagnetic wave propagating at frequencies which are below the cutoff frequency of the TM mode in the empty waveguide [18]. This is an example of wave propagation in a waveguide that provides negative permeability because the TM mode is below cutoff and the waveguide is loaded with a negative permittivity medium. It was shown in [19] that wave propagation in a MTM-loaded below-cutoff waveguide can be explained by the anisotropy of the SRR medium. The theory of a below-cutoff waveguide loaded by anisotropic MTMs was also presented in [20, 21].

In this paper we study a closed metallic waveguide of square cross-section loaded by metallic complementary SRRs (CSRRs). This waveguide may have an application as an interaction circuit for a vacuum electron device in which a rectilinear electron beam excites a TM-dominated mode with the longitudinal electric field in the direction of the electron velocity [13]. The CSRR is needed because it provides electric response for the longitudinal electric field [13]. In contrast to [13], in this paper we consider a different type of CSRR - planar complementary electric split ring resonators (CeSRRs) introduced in [22] and we present a simple model for a waveguide loaded by CeSRRs.

Using this example of a MTM-loaded waveguide we show that it is possible to determine the effective permittivity and permeability of the MTM, then fill the waveguide with this effective medium and predict the waveguide mode’s dispersion

properties by using the constitutive parameters of the effective medium. The effective constitutive parameters allow us to analyze the wave-beam interaction in the MTM-loaded waveguide.

In Section 2, we retrieve the effective constitutive parameters for a CeSRR MTM in free space using the existing method of MTM constitutive parameter retrieval [23-28]. In Section 3, we use the effective medium theory to study the dispersion characteristics of a cutoff metallic waveguide loaded by the CeSRRs. Then we compare the effective medium model with an HFSS simulation of an actual CeSRR loaded waveguide. In Section 4, we discuss the applications of the MTM-loaded waveguide in vacuum electron devices.

2. Complementary electric split ring resonators in free space

We first consider a MTM in free space, which consists of planar CeSRRs. It produces a "negative" electric response and not a "negative" magnetic response [22]. In this paper, we use a planar CeSRR, a schematic of which is shown in Fig. 1. The dimensions shown in Fig. 1 refer to a specific design to operate near 3 GHz. The CeSRR has some attractive advantages over the eSRR such as: greater symmetry that eliminates the magnetoelectric response which occurs in conventional SRRs; an all-metal construction to avoid dielectrics in vacuum; an enhanced transmission due to the resonance; and easy fabrication and assembly. If the dimension of the unit cell is much less than the wavelength λ, then the CeSRR MTM can be considered as an effective medium. Accordingly, we can retrieve the effective MTM constitutive parameters.

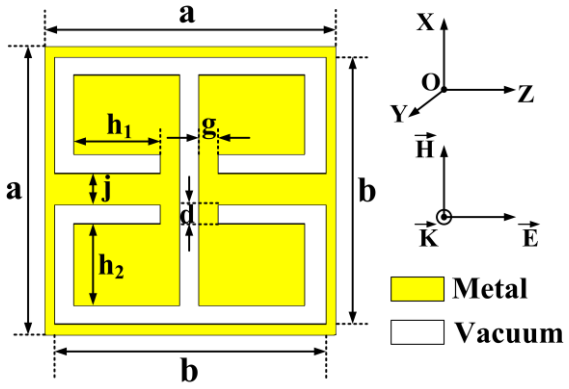

FIG. 1. The CeSRR unit cell used in this study. For operation near 3 GHz, the structural parameters (in mm) are a=14.5, b=13.5, d=1, j=1.5, h_1=4.25, h_2 =4, g=1, and thickness t=1 (not shown here).

As a specific example, we choose the dimensions of the unit cell as shown in Fig. 1. The periodic array of CeSRRs with the period *a* is perforated on a plate. Identical plates are set at distance *a* parallel to each other. We assume a plane wave propagating in the *y*-direction and with polarization in the *z*- direction, as shown in Fig. 1. The plane wave is normally incident on the CeSRR MTM surface. Here we do not consider the ohmic loss of the metal. Thus, the relative permittivity and permeability are only real.

We set up the HFSS model (a cubic geometry of size $a \times a \times a$) and use the driven-modal solver to obtain the S parameters. The amplitude and phase of the S parameters are shown in Fig. 2 (a) and (b), respectively. The resonant enhanced transmission at ~3 GHz results from circulating currents in the CeSRR and a pure electric response for the E_z polarization. The counter-circulating currents eliminate any magnetoelectric response [22].

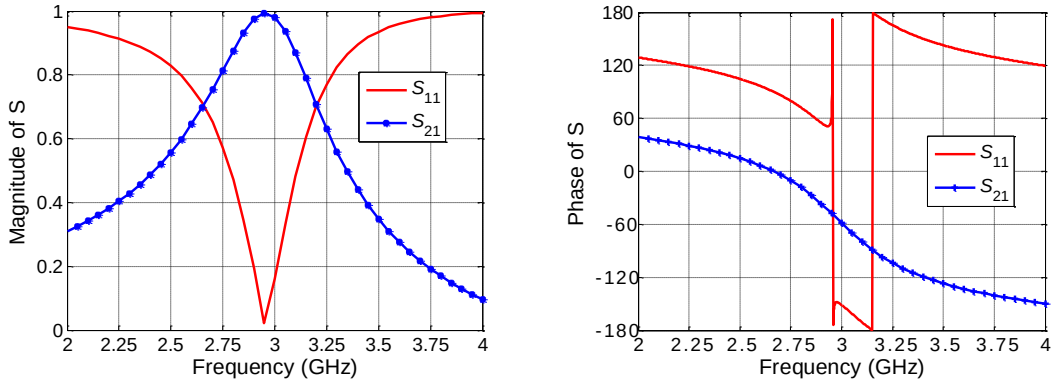

(a) (b)

FIG. 2. The amplitude (a) and the phase (b) of the scattering parameters *vs.* frequency.

We use the S parameter-based retrieval method [25] to retrieve the effective permittivity ε_{zz} and permeability μ_{xx}. The results are presented in Fig. 3(a). As noted in Ref. [22], the CeSRR permittivity is the sum of an effective Drude-like response (with an effective plasma frequency f_p =2.82 GHz for the structure of Fig. 1), arising from the interconnected metallic regions, and, at higher frequency, a Lorentz-like oscillator (with resonant frequency ~3.35 GHz for the structure of Fig. 1). As for the permeability, in fact, there is no magnetic response, as stated in [22, 28].

By changing the polarization of the incident wave from E_z to E_x (Fig. 1), we determine the S parameters and then retrieve the permittivity ε_{xx} and permeability μ_{zz}, as illustrated in Fig. 3(b).

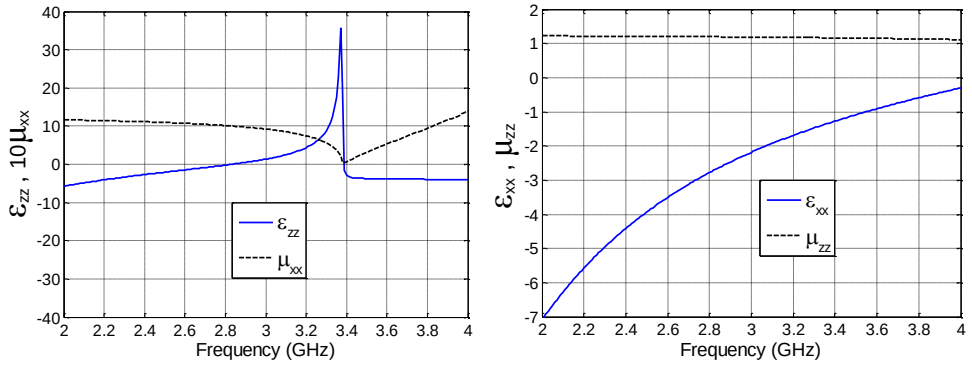

(a) (b)

FIG. 3. Retrieved permittivities and permeabilities of the CeSRRs as functions of frequency for *z* (a) and *x* (b) polarizations, respectively.

3. Complementary electric split ring resonator-loaded cutoff waveguide

A CeSRR-loaded cutoff waveguide is formed as follows. The CeSRR unit cell is periodically arranged along the *z*-axis to form a plate (the period is *a*), which is positioned in the middle of a square waveguide of cross-section $a \times a$, as shown in Fig. 4.

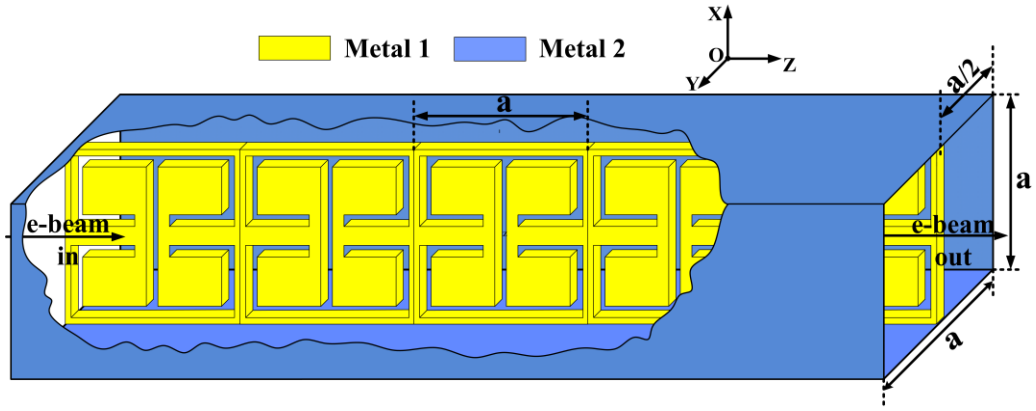

FIG. 4. The square metallic waveguide loaded with the CeSRR plate in the middle. Here *a*= 14.5 mm.

The square waveguide was simulated using the HFSS code. Figure 5(a) shows the longitudinal field E_z distribution in several axial slices of one period of the waveguide. The CeSRR is in the middle of the cell at $y=a/2$. The transverse distribution of the magnitude of $E_z(y)$ is plotted in Fig. 5(b) for the frequency of 3.07 GHz. The field is evanescent near the CeSRR plate and is zero at the wall. The walls (at $y=0$ and $y=a$) do not significantly affect the field distribution because the field amplitude and its derivative are small near the walls. In fact, the HFSS simulation of the dispersion characteristics indicates that the dispersion does not change when the E-wall boundary condition is changed to the H-wall boundary condition.

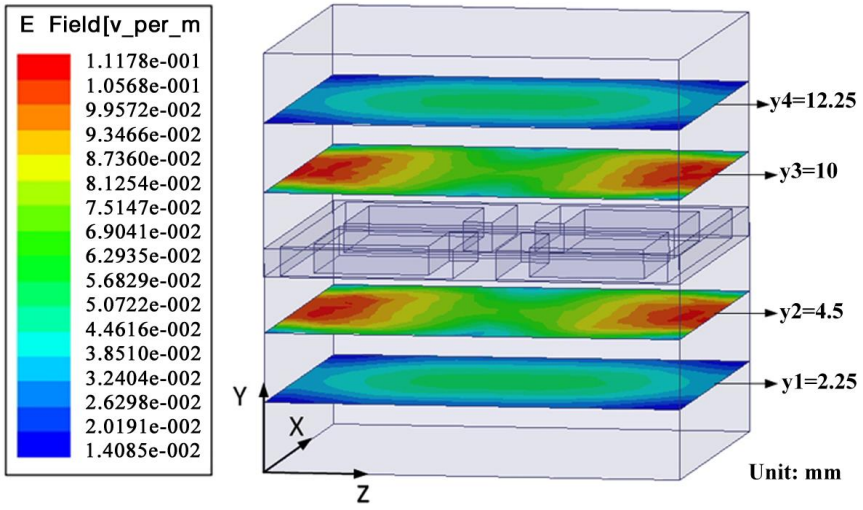

(a)

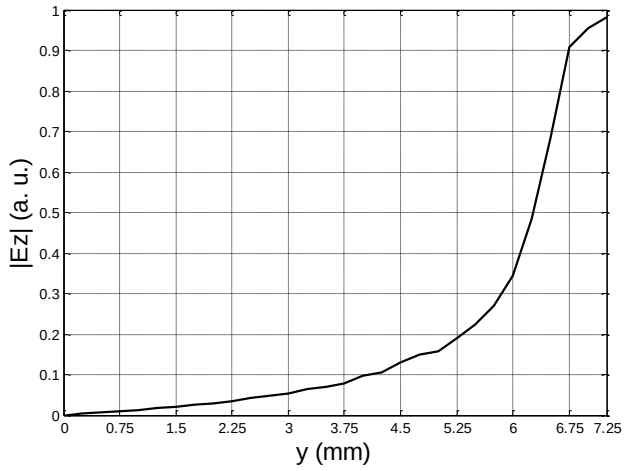

(b)

FIG. 5. The HFSS simulation of the square metallic waveguide loaded with the CeSRR plate in the middle at y=7.25 mm: (a) E_z field amplitude distribution in one cell at the slices parallel to the CeSRR at y=2.25, 4.5, 10, and 12.25 mm; (b) E_z field amplitude as a function of y; E_z is averaged over x.

In Section 2, the permittivity tensor of the medium consisting of a periodic set of CeSRR plates was determined. The MTM can be considered homogenized after the effective medium parameters are determined. A planar waveguide can be formed when the MTM is placed in between the metallic walls perpendicular to the CeSRR plates, *i.e.*, at x=0 and x=a. Therefore, one period of the MTM is placed in the x-direction. In the y-direction, the CeSRR plates are set periodically with the period a. The modes of this planar waveguide can be determined using the permittivity tensor and the metal wall boundary conditions.

3.1 Dispersion equation of a planar MTM-loaded waveguide

Now we formulate the wave equation for the modes of the planar waveguide filled with a homogeneous effective medium. We derive the dispersion equation for the TM mode assuming that the field does not depend on y, because the MTM is homogeneous.

The permittivity tensor is determined for the waves propagating perpendicular to the CeSRR plates. Therefore, it can be used to determine the waveguide modes close to cutoff. The effective permittivity is anisotropic and the permeability is isotropic, which leads to the following forms:

$$\bar{\bar{\varepsilon}} = \varepsilon_0 \begin{pmatrix} \varepsilon_{xx} & 0 & 0 \\ 0 & 1 & 0 \\ 0 & 0 & \varepsilon_{zz} \end{pmatrix}, \ \mu = \mu_0, \tag{1}$$

where ε_0 and μ_0 are the permittivity and permeability in vacuum, respectively.

Assuming an $e^{i\omega t}$ time dependence (ω is the angular frequency) and a source free CeSRR-loaded cutoff waveguide region, Maxwell's equations can be written as

$$\nabla \times \bar{E} = -i\omega\mu\bar{H}\,, \tag{2a}$$

$$\nabla \times \bar{H} = i\omega\bar{\bar{\varepsilon}} \bullet \bar{E}\,. \tag{2b}$$

Meanwhile, we assume that the wave propagates along the *z*-axis with an $e^{-i\beta z}$ dependence on *z*, where β is the phase constant. In addition, we suppose that the mode has a TM polarization. Inserting Eq. (1) into Eq. (2), making use of the separation of variables procedure, we derive the scalar wave equation for the E_z component as follows:

$$\left(\frac{\beta^2}{\omega^2\varepsilon_{xx}/c^2-\beta^2}+1\right)\frac{\partial^2 E_z}{\partial x^2}+\frac{\omega^2}{c^2}\varepsilon_{zz}E_z=0, \tag{3}$$

where *c* is the speed of light in free space. The boundary conditions can be applied directly to E_z:

$$E_z(x,z)=0, \quad \text{at} \quad x=0,a\,. \tag{4}$$

The resulting dispersion equation of the CeSRR-loaded cutoff waveguide can be expressed as:

$$\frac{(\pi/a)^2}{\varepsilon_{zz}}+\frac{\beta^2}{\varepsilon_{xx}}=\frac{\omega^2}{c^2}. \tag{5}$$

where ε_{zz} and ε_{xx} are dependent on ω.

3.2 Dispersion simulation

For the CeSRR-loaded sub-wavelength waveguide of Fig. 4, we have simulated the exact dispersion curve using the HFSS eigenmode solver and the result is the curve labeled "Simulation" in Fig. 6. We may also obtain the dispersion relation using the effective medium model, as described in Sec. 3.1 and Eq. (5). The resulting dispersion relation is shown in Fig. 6 as the "Theory" curve. Both approaches are in good qualitative agreement; both predict that the existing wave is a *backward* wave which results from the negative ε_{xx} and positive ε_{zz}, not a *forward* wave.

From this comparison of the HFSS simulation and the effective medium model we conclude that it is possible to retrieve the MTM constitutive parameters and predict the dispersion of the MTM-loaded waveguide. The retrieved ε_{xx} and ε_{zz} can be used in the dispersion equation (Eq. (5)) to calculate the dispersion of the mode close to cutoff when the phase advance is much smaller than π and the periodicity in the *z*-direction does not affect the dispersion.

3.3 Dispersion relation with fitted ε_{zz} and ε_{xx}

Good qualitative agreement is obtained between the dispersion relations of the effective medium model and the HFSS simulation. We can obtain better quantitative agreement by using fitted Drude models of the relative permittivities ε_{xx} *and* ε_{zz} in Eq. (5) using the form:

$$\varepsilon_{xx} = M_{xx}(1-\omega_{pxx}^2/\omega^2);\quad \varepsilon_{zz} = M_{zz}(1-\omega_{pzz}^2/\omega^2). \tag{6}$$

Here M_{xx} *and* M_{zz} are constants. The plasma frequencies are $\omega_{pxx}/2\pi$ = 4.2 GHz and $\omega_{pzz}/2\pi$ = 2.835 GHz. The constants selected for a best fit to the HFSS dispersion are M_{xx} =1.5 and M_{zz}=32. The result of calculating the dispersion relation, Eq. (5), using the relative permittivities of Eq. (6) is shown in Fig. 6 as the curve labeled "Fitting" This curve is in very good agreement with the HFSS simulation results.

Below a frequency of 3.0 GHz the guide wavelength ($\lambda_g = 2\pi/\beta$) is not very much larger than the unit cell size, which means the effective medium theory begins to deviate from the exact result. This fact is evidenced by the disagreement between the HFSS simulated dispersion curve and the dispersion curve using the fitting ε_{zz} and ε_{xx} as the phase advance exceeds π/2 (Fig. 6).

The *backward* mode is unidirectional; it can support a *fast* wave (left of the light line) and a *slow* wave (right of the light line) which is useful for vacuum electron devices.

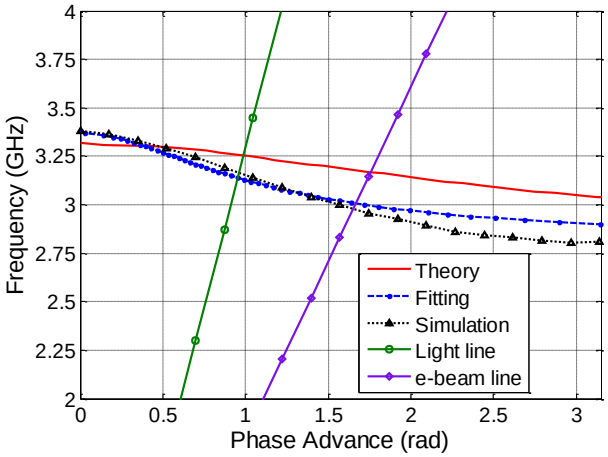

FIG. 6. Dispersion curves of Frequency *vs.* Phase Advance (βa) calculated by Simulation (HFSS),Theory (Eq. 5) and Fitting (Eqs. (5) and (6)). The dispersion curves are for the *backward* wave mode in the CeSRR-loaded square waveguide. The light line is $\omega=\beta c$ and the electron beam line is $\omega=\beta V$, where the frequency is $\omega/2\pi$, c is the velocity of light and V is the velocity of the electron beam.

4. Application in a vacuum electron device

The sub-wavelength MTM waveguide is suitable for a vacuum electron device. It can benefit vacuum electron devices where a small structure size is needed [13, 29].

We have shown that the simple model described by Eq. (5) is in agreement with the HFSS simulation of the MTM waveguide. The MTM waveguide mode can be excited by the rectilinear electron beam. The wave-beam interaction occurs in the vicinity of the intersection of the wave dispersion curve and the beam dispersion line $\omega=\beta V$, V is the velocity of the electron beam. In Fig. 6, the beam dispersion line is shown for the beam voltage of 100 kV.

4.1 Gain equation for effective medium theory

Using the effective medium permittivity tensor components ε_{zz} and ε_{xx} we determine the gain of the Cerenkov instability of the electron beam in the MTM waveguide [13]. The new longitudinal permittivity ε_{zzn} including the electron beam is given by [30]:

$$\varepsilon_{zzn} = \varepsilon_{zz} - \frac{\omega_b^2}{(\omega - \beta V)^2} \quad , \tag{7}$$

where the beam plasma frequency is determined by $\omega_b^2 = e^2 n_b / \varepsilon_0 m$; n_b is the electron density, e and m are the electron charge and mass respectively. The relativistic effects are not taken into account in this formulation. Eq. (5) thus can be rewritten as

$$\frac{(\pi / a)^2}{\varepsilon_{zzn}} + \frac{\beta^2}{\varepsilon_{xx}} = \frac{\omega^2}{c^2} . \tag{8}$$

From Eqs. (6) and (8) we derive the wave-beam interaction dispersion equation:

$$(\beta^2 - \beta_0^2)(\beta - \frac{\omega}{V})^2 = -\frac{\omega_b^2}{V^2}\frac{\pi^2}{a^2}\frac{\varepsilon_{xx}}{\varepsilon_{zz}^2} . \tag{9}$$

where β_0 is the solution of Eq. (8) with ω_b=0. Eq. (9) can be recognized as having the form of the dispersion relation of a traveling wave tube [31]. By neglecting interaction with the counter-propagating wave β=-β_0 and assuming no detuning from synchronism between the wave and the beam (β_0=ω/V) we determine the maximum of the imaginary part of the propagation constant:

$$\mathrm{Im}\,\beta = \frac{\sqrt{3}}{2}\frac{\omega}{V}(-\frac{\pi^2\omega_b^2 V^2}{2\omega^4 a^2}\frac{\varepsilon_{xx}}{\varepsilon_{zz}^2})^{1/3} . \tag{10}$$

Eq. (10) can be re-written for the gain G as

$$G = 2\,\mathrm{Im}\,\beta = \sqrt{3}\frac{\omega}{V}\left(-\frac{I}{I_0}2\pi^3\frac{c^3 V}{\omega^4 a^4}\frac{\varepsilon_{xx}}{\varepsilon_{zz}^2}\right)^{1/3} \quad , \tag{11}$$

where I_0=$4\pi\varepsilon_0 mc^3/e \approx 17$ kA.

4.2 Gain calculation using HFSS code

The gain in (Eq. (11)) was determined by using the effective medium representation of the CeSRRs to derive the dispersion relation. We may compare that result with a second, independent calculation of the gain using the HFSS code to calculate the wave-beam coupling impedance. The coupling impedance is then used in traveling wave tube theory to obtain the gain. The mean coupling impedance is represented as follows [31]:

$$\overline{K}_c = \frac{\frac{1}{S}\iint_s |E_z|^2 ds}{2\beta^2 P} \tag{12}$$

where P is the electromagnetic power propagating in the waveguide and E_z is the longitudinal electric field which is averaged over the electron beam cross-section ($S=a\times a$). The Pierce parameter C is determined by

$$C = \left(\frac{I\overline{K}_c}{4U}\right)^{1/3} \tag{13}$$

using the beam current I and the beam voltage U. The gain of the wave-beam instability is [31]

$$G = \sqrt{3}\frac{\omega}{V}C\,. \tag{14}$$

Fig. 7 shows a comparison of the gain calculation using the two approaches: the effective medium approach (Eq. (11)) versus a rigorous calculation using the exact fields calculated with the HFSS code. The gain is proportional to $I^{1/3}$, therefore, the ratio $G/I^{1/3}$ is plotted as a function of the frequency. The voltage U of the synchronous beam is varied with the frequency. The gain results of the simple effective medium theory model using the fitting parameters (Sec. 3.3) are in very good agreement with those of the HFSS simulation (Fig. 6). Meanwhile, Fig. 7 also shows the frequency tuning of the gain of the *backward* wave as the beam line ($\omega=\beta V$, see Fig. 6) varies with a change of voltage.

The Cerenkov instability of the electron beam in the MTM has specific features. The gain is higher as compared to a conventional Cerenkov electron device because the group velocity of the wave is lower. A *backward*-wave oscillator can be built based on this instability because the group velocity of the wave is *negative*.

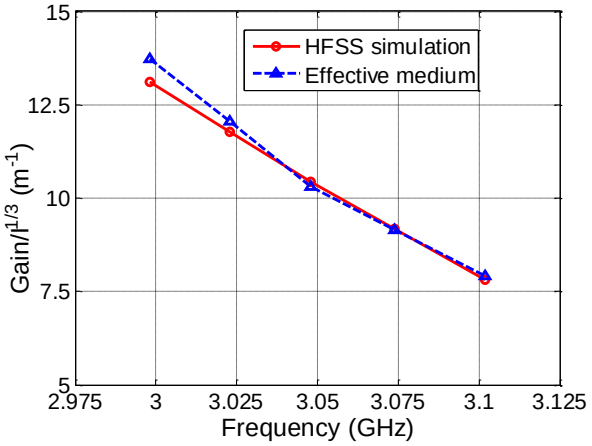

FIG. 7. Comparison of wave-beam instability Gain as a function of frequency between the HFSS simulation using Eq. (14) and the effective medium theory based on the fitting permittivity using Eq. (11). The current I is in Amperes.

5. Conclusion

We have characterized the CeSRR MTMs and proposed a CeSRR-loaded cutoff waveguide. The effective permittivity and permeability have been retrieved using the S parameter-based retrieval method for the CeSRR MTM in free space. Meanwhile, we have studied the wave propagation in a cutoff waveguide loaded by the CeSRRs using both theory and simulation. A backward wave mode has been found in the MTM loaded waveguide. The theoretical dispersion relation derived for the CeSRR MTM which is considered as an effective medium agrees qualitatively with the numerical simulation. Good agreement between the HFSS simulations and the effective medium model has been achieved by using the fitted permittivity tensor.

The interaction of the MTM waveguide wave with an electron beam has been studied. The coupling with the beam was calculated using HFSS and compared to the gain predicted by the effective medium model, with very good agreement. The effective medium approach is found to be useful for calculation of the modes of the waveguides loaded by the MTM. The gain of the wave-beam interaction in the MTM loaded waveguide can be analyzed using the effective medium parameters. This novel MTM structure may allow for the miniaturization of vacuum electron devices.

Acknowledgements

Work supported by AFOSR MURI Grant FA9550-12-1-0489 administered by the Univ. New Mexico; DOE, High Energy Physics (Grant No. DE-SC0010075); and the Natural Science Foundation of China (Grant Nos. 61471091 and 61125103).

References

[1] D. R. Smith, W. J. Padilla, D. C. Vier, S. C. Nemat-Nasser, and S. Schultz， Phys. Rev. Lett. **84**, 4184 (2000).

[2] V. G. Veselago, Sov. Phys. Usp. **10**, 509 (1968).

[3] G. Shvets, Phys. Rev. B **67**, 035109 (2003).

[4] Z. Y. Duan, C. Guo, and M. Chen, Opt. Express **19**, 13825 (2011).

[5] A. S. Gilmour, Jr. *Klystrons, Traveling Wave Tubes, Magnetrons, Cross-Field Amplifiers, and Gyrotrons* (Artech House, Boston-London, 2011).

[6] Y. M. Shin, G. S. Park, G. P. Scheitrum, and B. Arfin, IEEE Trans. Plasma Sci. **30**, 1317 (2003).

[7] C. L. Kory, M. E. Read, R. L. Ives, J. H. Booske, and P. Borchard, IEEE Trans. Electron Devices **56**, 713 (2009).

[8] Y. P. Bliokh, S. Savel'ev, and F. Nori, Phys. Rev. Lett. **100**, 244803 (2008).

[9] D. Shiffler, R. Seviour, E. Luchinskaya, E. Stranford, W. Tang, and D. French, IEEE Trans. Plasma Sci. **41**, 1679 (2013).

[10] M. I. Bakunov, R. V. Mikhaylovskiy, S. B. Bodrov, and B. S. Luk'yanchuk, Opt. Express **18**, 1684 (2010).

[11] D. Shiffler, J. Luginsland, D. M. French, and J. Watrous, IEEE Trans. Plasma Sci. **38**, 1462 (2010).

[12] Z. Y. Duan, C. Guo, J. Zhou, J. C. Lu, and M. Chen, Phys. Plasmas **19**, 013 (2012).
[13] M. A. Shapiro, S. Trendafilov, Y. Urzhumov, A. Alù, R. J. Temkin, and G. Shvets, Phys. Rev. B **86**, 085132 (2012).
[14] Z. Y. Duan, C. Guo, X. Guo, and M. Chen, Phys. Plasmas **20**, 093301 (2013).
[15] D. M. French, D. Shiffler, and K. Cartwright, Phys. Plasmas **20**, 083116 (2013).
[16] C. Caloz, C. C. Chang, and T. Itoh, J. Appl. Phys. **90**, 5483 (2001).
[17] R. Marqués, J. Martel, F. Mesa, and F. Medina, Phys. Rev. Lett. **89**, 183901 (2002) .
[18] J. Esteban, C. Camacho-Peñalosa, J. E. Page, T. M. Martín-Guerrero, and E. Márquez-Segura, IEEE Trans. Microw. Theory Tech. **53**, 1506 (2005).
[19] I. G. Kondratyev and A. I. Smirnov, Radiophys. Quant. Electronics **48**, 136 (2005).
[20] P. A. Belov and C. R. Simovski, Phys. Rev. E **72**, 036618 (2005).
[21] S. Hrabar, J. Bartolic, and Z. Sipus, IEEE Trans. Antenn. Propag. **53**, 110 (2005).
[22] H. T. Chen, J. F. O'Hara, A. J. Taylor, R. D. Averitt, C. Highstrete, M. Lee, and W. J. Padilla, Opt. Express **15**, 1084 (2007).
[23] D. R. Smith, S. Schultz, P. Markoš, and C. M. Soukoulis, Phys. Rev. B **65**, 195104 (2002).
[24] X. Chen, T. M. Grzegorczyk, B. I. Wu, J. Pacheco, and J. A. Kong, Phys. Rev. E **70**, 016608 (2004).
[25] D. R. Smith, D. C. Vier, Th. Koschny, and C. M. Soukoulis, Phys. Rev. E **71**, 036617 (2005).
[26] J. T. Costa, M. G. Silveirinha, and S. I. Maslovski, Phys. Rev. B **80**, 235124 (2009).
[27] Z. Szabó, G. H. Park, R. Hedge, and E. P. Li, IEEE Trans. Microw. Theory Tech. **58**, 2646 (2010).
[28] D. R. Smith, Phys. Rev. E **81**, 036605 (2010).
[29] Z. Y. Duan, B.I. Wu, S. Xi, H.S. Chen, and M. Chen, Prog. Electromagn. Res. Research **PIER 90**, 75 (2009).
[30] S. T. Ivanov, O. V. Dolgenko, and A. A. Rukhadze, J. Phys. A: Math. Gen. **8**, 585 (1975).
[31] S. E. Tsimring, *Electron Beams and Microwave Vacuum Electronics* (John Wiley and Sons, New Jersey, 2007).